

Electronic Supplementary Information

Strategies to Improve the Photovoltaic Performance of M-Series Acceptor-Based Polymer Solar Cells: Chemical Hybridization Versus Physical Blending of Acceptors
*Haiting Shi, †^{ab} Hui Guo, †^{ab} Dongdong Cai, ^a Jin-Yun Wang, ^a Yunlong Ma, ^{*a} and Qingdong Zheng ^{*c}*

^aState Key Laboratory of Structure Chemistry, Fujian Institute of Research on the Structure of Matter, Chinese Academy of Sciences, Fuzhou 350002, China. E-mail: mayunlong@fjirsm.ac.cn

^bCollege of Chemistry and Materials Science, Fujian Normal University, Fuzhou 350007, China.

^cState Key Laboratory of Coordination Chemistry, College of Engineering and Applied Sciences, Nanjing University, Nanjing 210023, China. E-mail: zhengqd@nju.edu.cn

†These authors contributed equally.

1. Materials and instruments

The polymer PM6 was purchased from Solarmer Materials Inc. [2-(9H-carbazol-9-yl) ethyl] phosphonic acid (2PACz) and 1,3,5-trichlorobenzene (TCB) was purchased from Tokyo Chemical Industry (TCI) Co., LTD. 2-(5,6,-difluoro-3-oxo-2,3-dihydro-1H-inden-1-ylidene)malononitrile (IC-2F) and 2-(5,6,-dichloro-3-oxo-2,3-dihydro-1H-inden-1-ylidene)malononitrile (IC-2Cl) were purchased from Nanjing Zhi Yan Technology Co. And other solvents and reagents were purchased from Sigma Aldrich Inc., Adamas-beta Ltd., Energy Chemical, and Tokyo Chemical Industry Co., Ltd. *etc.* All reagents and solvents were used directly without any further purification unless specified otherwise. ¹H NMR spectra were recorded at 400 MHz on a Bruker AVANCE III-400 spectrometer in CDCl₃ using tetramethyl silane as the internal standard. High-resolution mass spectroscopy (HRMS) measurements were performed on a UHR TOF LC/MS Mass Spectrometer. Ultraviolet-visible (UV-vis) absorption spectra of the neat films and the blend films were obtained from a spectrophotometer (Lambda 365 UV-vis). Photoluminescence (PL) were recorded by Edinburgh Instrument FLS 980 spectrometers at different excitation wavelengths for the corresponding films. The capacitance-frequency characteristics of the neat films and the blend films were measured by a LCR digital bridge (TH2827C). All the films used for UV-vis absorption spectroscopy, PL, and capacitance-frequency characterization measurements were thermally annealed at 85 °C for 5 minutes. Atomic force microscopy (AFM) was employed on a Bruker Nanoscope V station to record the surface morphology of the blend film by a peak force quantitative nanomechanical mode. Cyclic voltammetry

(CV) measurement was performed on a CHI 604E electrochemical workstation with a three-electrode cell in a nitrogen-bubbled 0.1 M tetrabutylammonium hexafluorophosphate (Bu_4NPF_6) solution in acetonitrile at a scan rate of 100 mV s^{-1} at room temperature. Platinum wire, Ag/AgNO₃ (0.1 M AgNO₃ in acetonitrile), and platinum plate were used as the counter electrode, reference electrode, and working electrode, respectively. The Ag/AgNO₃ reference electrode was calibrated using a ferrocene/ferrocenium redox couple as an external standard, whose oxidation potential is set at -4.82 eV with respect to zero vacuum level. The film samples were coated on the Pt plate electrode by dipping the electrode into corresponding solutions and then drying. The HOMO/LUMO energy levels of the materials were calculated according to the following equations:

$$E_{HOMO} = -(\varphi_{ox} + 4.82) \text{ (eV)} \quad (1)$$

$$E_{LUMO} = -(\varphi_{red} + 4.82) \text{ (eV)} \quad (2)$$

where φ_{ox} is the onset oxidation potential vs. Ag/AgNO₃ and φ_{red} is the onset reduction potential vs. Ag/AgNO₃.

2. Synthesis and characterization

Compound 1 was synthesized according to the reported method.^[S1]

Synthesis of compound 2: In a dry two neck round-bottomed flask, compound 1 (0.80 g, 0.737 mmol) was dissolved in 15 mL of 1,2-dichloroethane and placed under nitrogen atmosphere. The solution was cooled to 0 °C and stirred while phosphorus oxychloride (1.13 g, 7.37 mmol) and DMF (0.54 g, 7.37 mmol) were added under ice bath. After that, the mixture was stirred for 30 mins, then saturated potassium acetate solution was added and the reaction solution was extracted with dichloromethane. The combined organic layer was washed with water and brine, dried over anhydrous MgSO₄. After the removal of solvent, the residue was purified by column chromatography on silica gel using petroleum ether/dichloromethane (3:1) as the eluent, yielding compound 2 as an orange oil. (0.8 g, 95%). ¹H NMR (400 MHz, chloroform-d, δ) 9.92 (s, 1H), 7.70 (s, 1H), 7.24 (d, $J = 5.36$ Hz), 7.08 (d, $J = 5.24$ Hz, 1H), 4.72 (dd, $J_1 = 7.56$, $J_2 = 22.24$ Hz, 4H), 3.97 (dd, $J_1 = 7.08$, $J_2 = 11.56$ Hz, 4H), 2.14-0.63 (m, 92H). HRMS(MALDI) m/z: calcd. for C₆₇H₁₀₄N₂O₃S₄, 1112.6924; found,

1112.6891.

Synthesis of compound 3: Compound 2 (0.5 g, 0.448 mmol), 2-(5,6-difluoro-3-oxo-2,3-dihydro-1H-inden-1-ylidene) malononitrile (0.1 g, 0.448 mmol), 10mL toluene and pyridine (0.5 mL) were added to the flask under nitrogen and heated to reflux overnight. After the removal of solvent, the crude product was then purified by silica gel column using petroleum ether/dichloromethane (2:1 by volume) as the eluent. The pure product of compound 3 was obtained as blue oil (0.52 g, 88%). ¹H NMR (400 MHz, chloroform-*d*, δ) 8.92 (s, 1H), 8.47 (dd, $J_1=9.88$, $J_2=6.64$, 1H), 7.84 (s, 1H), 7.64 (t, $J=7.56$ Hz, 1H), 7.29 (d, $J=5.24$ Hz, 1H), 7.10 (d, $J=5.28$ Hz, 1H), 4.73 (dd, $J_1=22.60$, $J_2=9.24$ Hz, 5H), 4.01 (dd, $J_1=24.48$, $J_2=6.88$ Hz, 5H), 2.13-0.67 (m, 92H); ¹⁹F NMR (376 MHz, chloroform-*d*, δ) -124.21(d, $J=19.18$ Hz), -125.27(d, $J=19.18$ Hz). HRMS(MALDI) m/z: calcd. for C₇₉H₁₀₆F₂N₄O₃S₄, 1324.7114; found, 1324.7110.

Synthesis of compound 4: In a dry two neck round-bottomed flask, compound 3 (0.52 g, 0.737 mmol) was dissolved in 15 mL of 1,2-dichloroethane and placed under nitrogen atmosphere. The solution was cooled to 0 °C and stirred while phosphorus oxychloride (1.81 g, 11.60 mmol) and DMF (0.84 g, 11.60 mmol) were added successively, and then stirred for 12 h at 60 °C. After the reaction, Na₂CO₃ was added and the reaction solution was extracted with dichloromethane. The combined organic layer was washed with water and brine, dried over anhydrous MgSO₄. After the removal of solvent, the residue was purified by column chromatography on silica gel using petroleum ether/dichloromethane (2:1 by volume) as the eluent, yielding compound 4 as a dark blue solid. (0.55 g, 90%). ¹H NMR (400 MHz, chloroform-*d*, δ): 9.96 (s, 1H), 8.96 (s, 1H), 8.53 (dd, $J_1=9.68$, $J_2=6.28$ Hz, 1H), 7.90 (s, 1H), 7.73 (s, 1H), 7.68 (t, $J=7.24$ Hz, 1H), 4.75 (d, $J=7.40$ Hz, 4H), 4.01 (t, $J=7.84$ Hz, 4H), 2.11 (m, 2H), 1.72-0.87 (m, 94H); ¹⁹F NMR (376 MHz, chloroform-*d*, δ) -123.65 (d, $J=19.18$ Hz), -124.73 (d, $J=19.18$ Hz); HRMS (MALDI) m/z: calcd. for C₈₀H₁₀₆N₄O₄F₂S₄, 1352.7059; found, 1352.7023.

Synthesis of M36-FCl: Compound 4 (0.10 g, 0.074 mmol) and 2-(5,6-dichloro-3-oxo-2,3-dihydro-1H-inden-1-ylidene)malononitrile (0.019 g, 0.074 mmol) were dissolved in 10 mL of toluene, and 0.2 mL of acetic anhydride and 0.1 mL of boron

trifluoride diethyl ether were added sequentially after the reactant was fully dissolved. The reaction was carried out for 30 mins at room temperature. At the end of the reaction, the reaction mixture was poured into methanol and the precipitate was filtered off. The crude product was then purified by silica gel column using petroleum ether/dichloromethane (1:1, v/v) as the eluent, yielding M36-FCI as a black solid (0.08 g, 70%). ¹H NMR (400 MHz, chloroform-*d*, δ) 8.97 (s, 1H), 8.95 (s, 1H), 8.73 (s, 1H), 8.51 (dd, $J_1= 10.00$, $J_2=6.48$ Hz, 1H), 7.93 (s, 1H), 7.89 (s, 2H), 7.68 (t, $J = 7.48$ Hz, 1H), 4.74 (d, $J = 7.64$ Hz, 4H), 4.02 (d, $J = 6.84$ Hz, 4H), 2.11-0.67 (m, 92H); ¹⁹F NMR (376.4 MHz, chloroform-*d*) δ -123.30 (dd, $J_1= 10.16$ Hz, $J_2 = 19.10$ Hz), -124.39 (dd, $J_1= 10.08$, $J_2= 19.18$ Hz); HRMS (MALDI) *m/z*: calcd. for C₉₂H₁₀₈N₆Cl₂O₄F₂S₄, 1596.6655; found, 1596.6603.

3. Solar cell fabrication and characterization

Solar cells were fabricated with a device structure of ITO/2PACz/active layer/PDIN/Ag. 2PACz monolayer was prepared according to the method published by Lin *et al.*^[S2] The monolayer of 2PACz (0.5 mg/mL in ethanol) was firstly deposited on the top of the cleaned ITO glass substrates at 3000 rpm for 30 s, followed by thermal annealing at 50 °C for 4 min in a N₂-filled glovebox. For the bulk heterojunction films, the PM6:M36-FCI was dissolved in chlorobenzene (CB) solution with a D:A weight ratio of 1:1 and total concentration of 18 mg mL⁻¹, the PM6:M36F:M36Cl was prepared in CB with a D:A₁:A₂ weight ratio of 1:0.5:0.5 and total concentration of 18 mg mL⁻¹. Trichlorobenzene (TCB) at 10 mg/mL was added as an additive prior to spin-coating process.^[S3] The blend solutions were cooled to room temperature (25 °C) before used, and then were spin-coated on the top of the 2PACz layer to maintain an optimal thickness of 110 nm. The acceptor devices were fabricated with a structure of ITO/PEDOT:PSS/M36-FCI or M36F:M36Cl (with a ratio of 1:1) /PDIN/Ag. The filtered PEDOT:PSS solution (Baytron PVP AI 4083 from H. C. Starck) was spin-coated onto the cleaned ITO substrates at 3500 rpm for 30 s, followed by baking at 140 °C for 15 min in air. Subsequently, the PEDOT: PSS-coated ITO glass substrates were transferred into a N₂-filled glovebox. The optimized M36-FCI and M36F:M36Cl films

with approximately 85 nm are obtained by spin-coating M36-FCl and M36F:M36Cl chloroform solutions (22 mg mL^{-1}) at 3000 rpm for 40 s. After film formation, all the active layers were thermally annealed at $85 \text{ }^\circ\text{C}$ for 5 minutes. Successively, PDIN methanol solution (2.0 mg/mL) was spin-coated on the active layer at 3000 rpm for 30 s to afford a buffer layer with a thickness of ca. 10 nm. Finally, 120 nm of Ag top electrode was deposited onto the PDIN buffer layer through shadow masks by thermal evaporation at a pressure of $1.0 \times 10^{-4} \text{ Pa}$. The active area of the devices is 4.15 mm^2 .

To study the charge generation and dissociation processes of the photovoltaic devices, plots of the J_{ph} versus V_{eff} of the PSCs were measured. Here, J_{ph} and V_{eff} are defined as $J_{\text{ph}} = J_{\text{L}} - J_{\text{D}}$ and $V_{\text{eff}} = V_0 - V_{\text{appl}}$, respectively, where J_{D} and J_{L} are the photocurrent densities in the dark and under the illumination, and V_{appl} is the applied bias voltage and V_0 is the voltage at which $J_{\text{ph}} = 0$, respectively. Usually, V_{eff} determines the electric field in the bulk region and thereby determines the carrier transport and the photocurrent extraction. At high V_{eff} values, charge carriers rapidly move toward the related electrodes with minimal recombination. The J_{ph} reaches the saturation current density (J_{sat}) at high V_{eff} ($\geq 2.0 \text{ V}$ in these cases).

The current density-voltage (J - V) characteristics were measured using a Keithley 2400 Source-Measure Unit. An Oriel Sol3A simulator (Newport) was used as a light source. The light intensity was calibrated to 100 mW cm^{-2} by a NREL certified silicon reference cell. EQE data were taken by using the QE/IPCE measurement kit (QE-PV-SI) from Newport.

4. Hole- and electron-only device fabrication and characterization

The space-charge-limited current (SCLC) method was used to study the charge transport properties of the blend film. The hole-only devices were fabricated with an architecture of ITO/PEDOT: PSS/active layer/ MoO_3 /Ag, while electron-only devices were fabricated with an architecture of ITO/ ZnO /active layer/PDIN/Al. The active layers were prepared using the same method as that used for the best-performance solar cells. The device area was fixed at 4.15 mm^2 . The current density (J) was measured by a Keithley 2400 source measurement unit. The SCLC hole/electron mobilities were

calculated according to the following equation:

$$J = \frac{9\varepsilon_r\varepsilon_0\mu V^2}{8L^3} \quad (3)$$

where J is the current density (A m^{-2}), ε_0 is the free-space permittivity ($8.85 \times 10^{-12} \text{ F m}^{-1}$), ε_r is the relative dielectric constant of the active layer material (usually 2-4 for organic semiconductors, herein we used a relative dielectric constant of 3), μ is the mobility of hole or electron, V is the voltage drop across the SCLC device ($V = V_{app} - V_{bi}$, where V_{app} is the applied voltage to the device and V_{bi} is the built-in voltage due to the difference in the work function of two electrodes), and L is the thickness of the active layer. The thickness of the film was determined by a Bruker Dektak XT surface profilometer. In this work, the active layer thicknesses of the PM6:M36-FCI- and PM6:M36F:M36Cl-based hole-only devices are 95 nm and 93 nm, respectively; while those for the PM6:M36-FCI- and PM6:M36F:M36Cl-based electron-only devices are 92 nm and 90 nm, respectively. The hole- or electron-mobility can be calculated from the slope of the $J^{1/2}$ - V curves.

5. GIWAXS characterization

The 2D GIWAXS/GISAXS patterns were acquired using a XEUSS SAXS/WAXS system at the Fujian Science & Technology Innovation Laboratory for Optoelectronic Information of China. All samples for GIWAXS and GISAXS measurements were prepared on the PEDOT:PSS-coated Si substrates using the same method as that used for the best-performance OSCs fabrication. The wavelength of the X-ray beam is 1.54 Å, and the incident angle was set as 0.2°. Scattered X-rays were detected by using a Dectris Pilatus 300 K photon counting detector.

6. GISAXS modelling

The objective is to measure and compare the phase separation in PM6: NFAs blends. A universal model expressed in Equation 4 was used to fit the 1D GISAXS profiles using the fitting software Sas View (Version 5.0.6). The first term of the equation is the so-called Debye-Anderson-Brumberger (DAB) term, where q is the scattering wave vector, A is an independent fitting parameter, and ξ is the average

correlation length of the intermixing phase. The Fractal model is the second term of the equation, which means that the NFAs are occupied with a fractal-like structure. The form factor of primary crystalline particles (as measured by the spherical shape of radius R here) is related to $P(q, R)$. The interaction between primary particles in this fractal-like aggregation system is described by $S(q, R)$, which is the fractal structure factor. $P(q, R)$ includes the product of particle volume fraction, the square of scattering length density difference between crystalline and amorphous polymers $\Delta\rho^2$ and crystalline particle volume V_p . $S(q)$ is given by Equation 5. The correlation length and the fractal dimension of the fractal-like acceptor aggregates are represented by η and D , respectively. R is the mean radius of primary crystalline particles. The Guinier radius (R_g) is used to characterize the average domain size of the acceptor phase (see Equation 6). The incoherent scattering background is the cause of the constant C .

$$I(q) = \frac{A}{[1 + (q\xi)^2]^2} + B(P(q,R))S(q,R,\eta,D) + C \quad (4)$$

$$S(q) = 1 + \frac{D\Gamma(D-1) \sin[(D-1)\tan^{-1}(q\eta)]}{[1 + 1/(q\eta)^2]^{(D-1)/2} (qR)^D} \quad (5)$$

$$R_g = \sqrt{\frac{D(D+1)}{2}}\eta \quad (6)$$

7. Dielectric-properties studies

The dielectric constants of the neat films and the blend films were determined by the capacitance-frequency measurements with a device structure of Al/the neat films or the blend films/Al under the frequency from 20 Hz to 1.0×10^6 Hz. The dielectric constant was evaluated by the material's geometric capacitance.^[S4] When the geometric

capacitance was found, the value was calculated by the equation of $\varepsilon = \frac{C_g d}{\varepsilon_0 A}$,^[S5] where the C_g is the geometric capacitance, d is the thickness of the active layer, ε_0 is the vacuum permittivity with the value of 8.85×10^{-12} F/m, and A is the contact area. The active layer area of the device is 0.09 cm^2 .

8. Temperature-dependent photoluminescence spectra measurements

To demonstrate the contribution of improved ϵ_r to E_a , we conducted a temperature-dependent photoluminescence (PL) spectrum to obtain the experimental E_a . The M36-FCl and M36F:M36Cl solution (15 mg mL⁻¹) was prepared in chloroform, and the thin-film samples were prepared *via* spin-coating the solution onto the quartz substrate. Temperature-dependent PL spectra were measured by Edinburgh Instrument FLS 980 multi-function fluorescence spectrometers with excitation at the wavelength of 750 nm for M36-FCl and M36F:M36Cl provided by ozone-free continuous xenon lamp. Thermal quenching of PL emission intensity was observable from 80 to 300 K. The E_a was calculated by fitting the integrated PL emissions as a function of temperature according to Arrhenius equation^[S6-S7]:

$$I(T) = \frac{I_0}{1 + A \exp\left(-E_a/k_B T\right)} \quad (7)$$

where I_0 is the intensity at 0 K, k_B is the Boltzmann constant, and T is the temperature.

9. Additional Tables and Figures

Table S1. The relative dielectric constants of the M36-FCl, M36F: M36Cl, PM6: M36-FCl, and PM6:M36F:M36Cl films.

Samples	ϵ_r ^[a]
M36-FCl	4.85±0.15
M36F:M36Cl	3.01±0.08
PM6:M36-FCl	3.94±0.09
PM6:M36F:M36Cl	3.04±0.22

^[a]The means with deviations are calculated from the dielectric constants in the frequency range of 10³-10⁵ Hz.

Table S2. Summary of optimized devices based on M36-FCl and M36F:M36Cl films.

Acceptors	V_{oc} (V)	J_{sc} (mA/cm ²)	FF (%)	PCE (%) ^[a]
M36-FCl	0.899	0.157	30.49	0.043 (0.039±0.003)
M36F:M36Cl	0.930	0.098	36.79	0.033 (0.030±0.002)

^[a]In parentheses are average values based on 8 devices.

Table S3. Photovoltaic properties of PSCs based on PM6:M36-FCl with different annealing temperatures and time.^[a]

Temperature (°C)	Time(min)	V_{oc} (V)	J_{sc} (mA/cm ²)	FF (%)	PCE ^[b] (%)
without	0	0.906	25.10	76.36	17.36 (17.21±0.12)
80	5	0.901	25.78	78.06	18.13 (18.03±0.07)
85	5	0.900	26.35	78.03	18.51 (18.32±0.09)
90	5	0.895	25.99	78.44	18.26 (18.13±0.11)
85	3	0.900	26.22	77.80	18.35 (18.21±0.13)
85	7	0.894	26.27	77.47	18.19 (18.05±0.10)

^[a]The PM6:M36-FCl (1:1 by weight) were added trichlorobenzene at 10 mg/mL as the additive;

^[b]The average PCEs with standard deviations in the parentheses are based on 8 devices.

Table S4. Photovoltaic properties of BHJ PSCs based on PM6: M36-FCl with different concentration of the TCB additive.^[a]

TCB (mg/ml)	V_{oc} (V)	J_{sc} (mA/cm ²)	FF (%)	PCE ^[b] (%)
0	0.910	24.99	74.95	17.05 (16.87±0.11)
5	0.900	26.32	77.43	18.35 (18.15±0.11)
10	0.900	26.35	78.03	18.51 (18.32±0.09)
15	0.892	26.29	76.86	18.04 (17.93±0.07)

^[a]The PM6:M36-FCl blends (1:1 by weight) were annealed at 85 °C for 5 min; ^[b]The average PCEs with standard deviations in the parentheses are based on 8 devices.

Table S5. Photovoltaic properties of BHJ PSCs based on PM6: M36-FCl with different concentration of the 1-chloronaphthalene (CN) additive.

CN (vol %)	V_{oc} (V)	J_{sc} (mA/cm ²)	FF (%)	PCE ^[b] (%)
0	0.910	24.99	74.95	17.05 (16.87±0.11)
0.25	0.902	25.90	74.63	17.43 (17.21±0.10)
0.5	0.897	25.84	77.97	18.07 (17.96±0.05)
1	0.884	25.85	77.99	17.83 (17.71±0.09)

^[a]The PM6:M36-FCI blends (1:1 by weight) were annealed at 85 °C for 5 min; ^[b]The average PCEs with standard deviations in the parentheses are based on 8 devices.

Table S6. Statistical sheet of PCE versus FF of linear ADA-type NFA-based organic solar cells with PCE > 12% ever reported.

Acceptor	Donor	PCE (%)	FF (%)	Ref.
M36-FCI	PM6	18.51	78.0	This work
SN6C9-4F	PBDB-T	12.07	68.7	<i>Chin. J. Chem.</i> 2025 , <i>43</i> , 13.
TBB	PBQx-TF	16.2	74.0	<i>CCS Chem.</i> 2024 , doi: 10.31635/ccschem.024.202303631.
C-F	D18	15.4	77.2	<i>ACS Mater. Lett.</i> 2024 , <i>6</i> , 2100.
S-F	D18	17.0	77.1	
PTBTT-4F	PM6	14.50	75.6	<i>Small</i> 2024 , <i>20</i> , 2305529.
PTBTT-4Cl	PM6	14.03	72.5	
TPBTT-4F	PM6	15.72	74.2	
TPBTT-4Cl	PM6	14.85	68.5	
DMT-HF	PM6	17.17	72.9	<i>Angew. Chem. Int. Ed.</i> 2024 , doi: 10.1002/anie.202411155.
M36:PW-Se	PM6	18.00	77.3	<i>Adv. Mater.</i> 2024 , <i>36</i> , 2314169.
M36	PM6	18.2	78.1	<i>Adv. Energy Mater.</i> 2024 , <i>14</i> , 2401816.
MC7F3	PM1	17.61	79.5	<i>Chem</i> 2024 , <i>10</i> , 3131.
IMC8-4Cl	D18	13.99	62.5	<i>ACS Mater. Lett.</i> 2024 , <i>6</i> , 2100.
BDOTP-1	D18-B	16.93	72.4	<i>Carbon Energy</i> 2023 , <i>5</i> , e250.
BDOTP-2	D18-B	15.48	71.1	
ZITI-N-6F	D18	16.11	73.8	<i>Fundam. Res.</i> 2023 , doi:10.1016/j.fmre.2023.03.010.
ZITI-N-6F/ ZITI-N-8F	D18	17.09	75.9	
ZITI-N-8F	D18	15.20	73.6	
MD1T	PBDB-T	12.43	68.0	<i>Aggregate</i> 2023 , <i>4</i> , e322.
M36	PM6	17.02	78.4	<i>Nano Energy</i> 2023 , <i>107</i> , 108116.
MQ1- δ	PM6	12.08	63.3	<i>Chin. Chem. Lett.</i> 2023 , <i>34</i> , 108448.
ThPy6	PM6	16.11	78.9	<i>Adv. Funct. Mater.</i> 2022 , <i>32</i> , 2203200.
IDTP-4F	PM6	15.02	75.7	<i>Chem. Eng. J.</i> 2022 , <i>427</i> , 131674.
TIT-2FIC	PM6	13.00	69.4	
ThPy2	PM6	12.30	73.8	<i>Natl. Sci. Rev.</i> 2022 , <i>9</i> , nwac076.
ThPy3	PM6	15.30	77.1	
PTBTTP-4F	PBDB-T	12.33	69.0	<i>Org. Electron.</i> 2022 , <i>103</i> , 106461.
2PIC	PM6	12.60	67.3	<i>Chin. J. Chem.</i> 2022 , <i>40</i> , 2861.
M14	PM6	16.46	76.6	<i>CCS Chem.</i> 2022 , <i>5</i> , 455.
M17	PM6	13.01	69.4	
MQ7-i	PM6	16.23	74.4	<i>J. Mater. Chem. A</i> 2022 , <i>10</i> , 23915.
cis-MF	J71	12.31	67.0	<i>Chem. Eng. J.</i> 2022 , <i>432</i> , 134393.

ML-2FM	PM6	15.33	73.4	<i>Solar RRL</i> 2022 , 6, 2200119.
MC1	PM6	12.02	64.8	<i>Chem. Eng. J.</i> 2022 , 427, 131022.
MS1	PM6	15.01	74.1	
M3	PM6	16.66	76.2	<i>Joule</i> 2021 , 5, 197.
M6	PM6	15.45	70.3	<i>Adv. Funct. Mater.</i> 2021 , 31, 2010436.
MQ5:M36	PM6	17.24	76.0	<i>ACS Appl. Mater. Interfaces</i> , 2021 , 13, 57684.
M13	PM6	13.14	67.0	<i>Chem. Eng. J.</i> 2021 , 418, 129497.
MQ3	PM6	13.51	66.9	
MQ5	PM6	15.64	74.3	<i>Angew. Chem. Int. Ed.</i> 2021 , 60, 19314.
MQ6	PM6	16.39	75.7	
IT4F	PFBCPZ	15.3	78.5	<i>Nano Energy</i> 2021 , 82, 105679.
DTTC-4Cl	T1	14.43	76.3	
DTSiC-4Cl	T1	14.46	73.6	<i>Solar RRL</i> 2020 , 4, 2000357.
DTTC-4F	PM6	13.89	67.6	
DTTC-4Cl	PM6	15.42	74.0	<i>J. Mater. Chem. A</i> 2020 , 8, 1131.
DTC-4F	PM6	13.37	70.4	
4TCIC-4F	PM7	13.02	73.0	<i>Solar RRL</i> 2020 , 4, 1900417.
IPTBO-4Cl	PM6	15.00	72.6	
IPT-4F	PM6	14.96	74.2	<i>J. Mater. Chem. A</i> 2020 , 8, 5458.
IDTP-4F	PM7	15.20	74.6	<i>Adv. Funct. Mater.</i> 2020 , 30, 2000383.
TPIC-4Cl	PM7	15.31	75.5	<i>J. Mater. Chem. A</i> 2020 , 8, 5927.
P6IC	PTB7-Th	12.20	70.2	<i>ACS Appl. Mater. Interfaces</i> 2020 , 12, 14029.
M4	PM6	14.75	71.5	<i>J. Mater. Chem. A</i> 2020 , 8, 24543.
M34	PM6	15.24	70.7	<i>Angew. Chem. Int. Ed.</i> 2020 , 59, 21627.
M36	PM6	16.00	72.1	<i>Natl. Sci. Rev.</i> 2020 , 7, 1886.
ZITI-N	J71	13.68	72.0	
ZITI-C	J71	13.18	72.7	<i>iScience</i> 2019 , 19, 883.
CZTT-4F	PM6	12.07	65.1	<i>J. Mater. Chem. A</i> 2019 , 7, 21903.
IT4F	T1	15.1	78.0	<i>Adv. Mater.</i> 2019 , 31, 1808356.
IPIC-4Cl	PBDB-T	13.40	74.0	<i>Adv. Funct. Mater.</i> 2019 , 29, 1903269.
INPIC-4F	PBDB-T	13.13	71.5	<i>Adv. Mater.</i> 2018 , 30, 1707150.
SN6IC-4F	PBDB-T	13.20	73.0	<i>Chem. Mater.</i> 2018 , 30, 5429.

Table S7. Photovoltaic properties of PSCs based on PM1:M36-FCl and D18:M36-FCl.

BHJ	V_{oc} (V)	J_{sc} (mA/cm ²)	FF (%)	PCE (%) ^[a]
PM1:M36-FCl	0.881	24.41	74.54	16.03 (15.96±0.09)

D18:M36-FCI	0.868	25.96	76.77	17.30 (17.19±0.16)
-------------	-------	-------	-------	--------------------

^[a]In parentheses are average values based on 8 devices.

Table S8. Photovoltaic properties of inverted PSCs based on the PM6:M36-FCI and PM6:M36F:M36Cl blend.

Active layer	V_{oc} [V]	J_{sc} [mA/cm ²]	FF [%]	PCE [%] ^[a]
PM6: M36-FCI	0.842	24.62	73.03	15.30 (15.18±0.10)
PM6:M36F:M36Cl	0.839	24.27	73.35	14.95 (14.81±0.15)

^[a]The average PCEs with standard deviations in the parentheses are based on 8 devices.

Table S9. All lifetimes relevant to the assessment of exciton dissociation efficiency obtained using time-resolved photoluminescence (TRPL) measurements.

Sample	τ_0 (ns) ^[a]	Blends	τ_q (ns) ^[b]	τ_d (ns) ^[c]	η_d (%) ^[d]
M36-FCI	1.10	PM6: M36-FCI	0.31	0.43	72
M36F:M36Cl	1.00	PM6:M36F:M36Cl	0.33	0.51	66

^[a] τ_0 represents singlet exciton lifetime; ^[b] τ_q represents lifetime of fluorescence quenching in the BHJ; ^[c] τ_d represents lifetime of exciton dissociation in the BHJ, which is calculated using Equation

$$\tau_d = \frac{1}{\frac{1}{\tau_q} - \frac{1}{\tau_0}}$$
 of τ_q τ_0 ; ^[d] η_d represents exciton dissociation efficiency in the BHJ, which is calculated

using Equation of
$$\eta_d = \frac{\frac{1}{\tau_d}}{\frac{1}{\tau_d} + \frac{1}{\tau_0}}$$

Table S10. The parameters of diffraction peaks from GIWAXS line-cuts of out-of-plane and in-plane profiles.

Samples	π - π stacking		lamellar stacking	
	$d_{\pi-\pi}$ [Å] ^[a]	CCL [Å] (FWHM) ^[b]	d_l [Å] ^[a]	CCL [Å] (FWHM) ^[b]
M36-FCI	3.76	16.38 (0.345 Å ⁻¹)	21.51	95.80 (0.059 Å ⁻¹)
M36F:M36Cl	3.80	21.74 (0.260 Å ⁻¹)	21.14	79.61 (0.071 Å ⁻¹)
PM6:M36-FCI	3.85	22.34 (0.253 Å ⁻¹)	21.66	94.20 (0.06 Å ⁻¹)
PM6:M36F:M36Cl	3.85	20.70 (0.273 Å ⁻¹)	21.66	80.74 (0.07 Å ⁻¹)

[a]The (010) diffraction peak along the q_z axis, and the (100) diffraction peak along the q_{xy} axis;

[b]The crystal coherence length (CCL) estimated from the Scherrer equation ($CCL=2\pi K/FWHM$, $K=0.9$), where FWHM is the full width at half maximum of the diffraction peak.

Table S11. Morphology parameters fitted by GISAXS profiles.

Blend film	ξ (nm)	$2R_g$ (nm)
PM6:M36-FCl	11.61	12.06
PM6:M36F:M36Cl	16.79	11.04

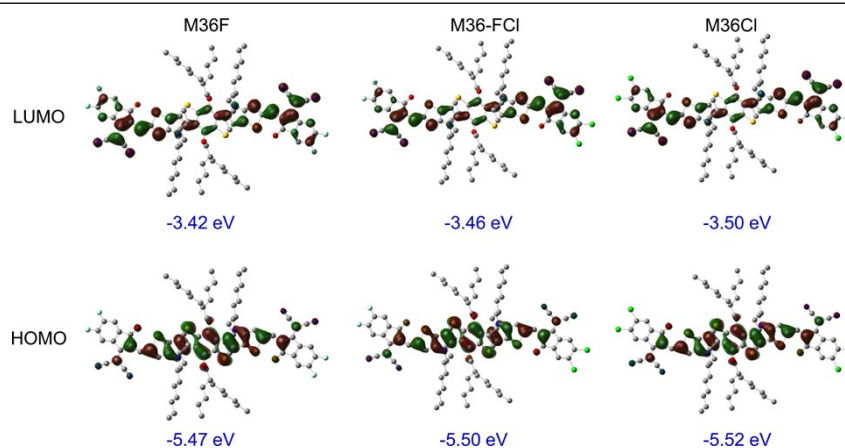


Fig. S1 Calculated HOMO and LUMO energy levels of M36F, M36Cl and M36-FCl.

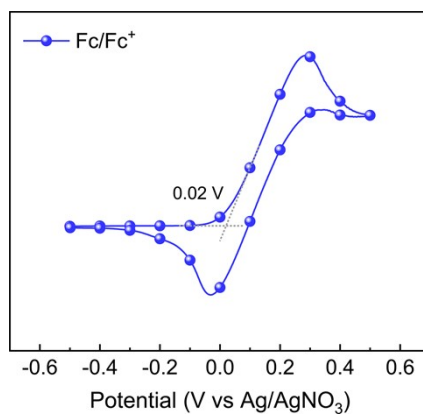


Fig. S2 The cyclic voltammogram of the ferrocene/ferrocenium (Fc/Fc⁺) couple.

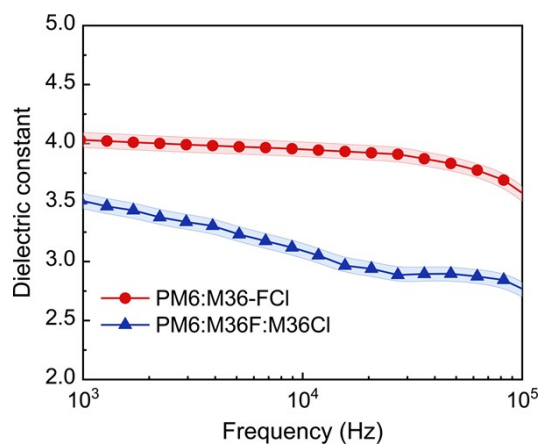


Fig. S3 Capacitance versus frequency plots for the PM6:M36-FCl and PM6:M36F:M36Cl films.

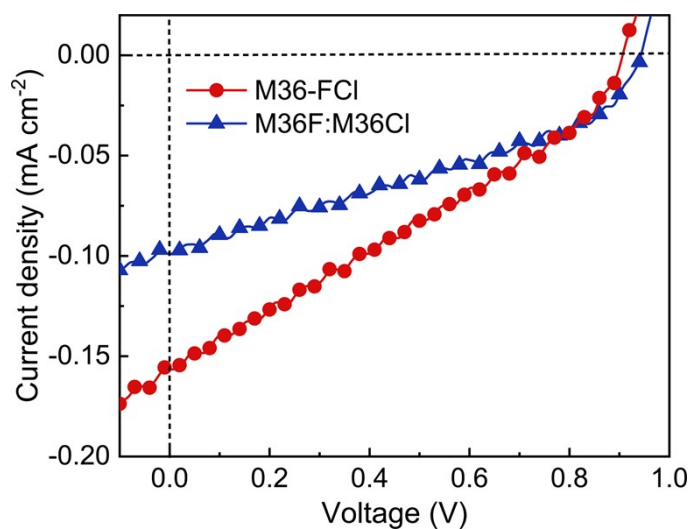


Fig. S4 J - V curves of the organic solar cells based on M36-FCl and M36F:M36Cl films.

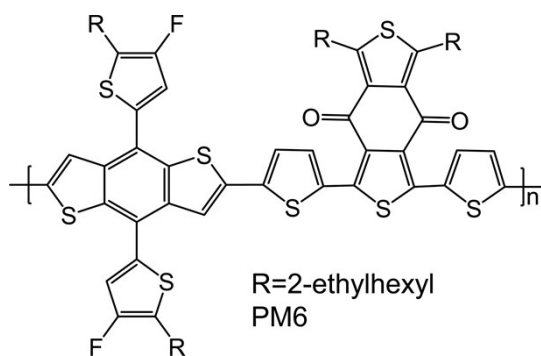


Fig. S5 Chemical structure of PM6.

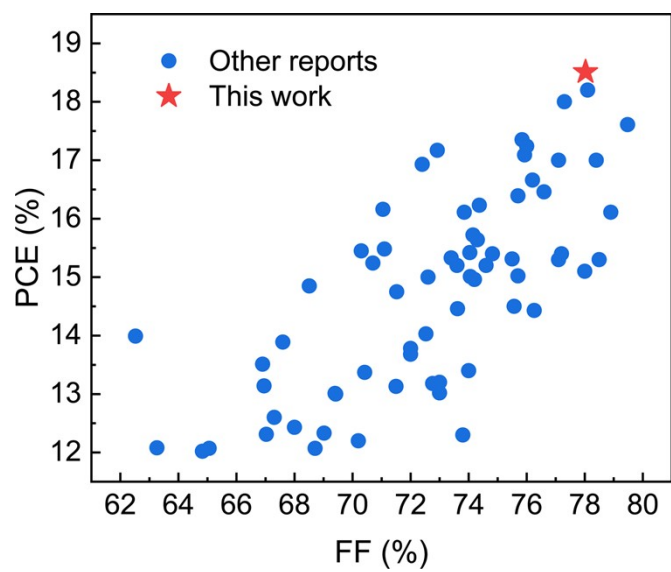


Fig. S6 The PCE-FF data of organic solar cells based on linear ADA-type NFAs reported in recent years.



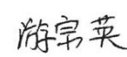




Fig. S7 The certification test report of the best performance provided by National Photovoltaic Product Quality Inspection & Testing Center (Report cover).

Chengdu Institute of Product Quality Inspection Co., Ltd.
National Photovoltaic Product Quality Inspection & Testing Center
TEST REPORT

Test Report No. AGXB124W00743

Page 1 of 2

Product Name	M36-FC1	Trade Mark	/	
Manufacture Date	20/11/2024	Model /Type	Mask-3.74 mm ²	
Sample No.	AGXB124W00743	Sample Grade	/	
Sample Quantity	One piece	Sample State	/	
Delivery Date	21/11/2024	Sample Delivered personnel	Dongdong Cai	
Commission unit	Fujian Institute of Research on the Structure of Matter, Chinese Academy of Sciences	Manufacturer	Fujian Institute of Research on the Structure of Matter, Chinese Academy of Sciences	
Commission unit address	No. 155, Yangqiao Road West, Fuzhou, Fujian, P. R. China	Manufacturer Address	No. 155, Yangqiao Road West, Fuzhou, Fujian, P. R. China	
Commission unit Zip code	350002	Manufacturer Zip code	350002	
Commission unit Tel.	15396061345	Manufacturer Tel.	15396061345	
Center Address	No. 355, 2 nd Tengfei Road, Southwest Airport Economic Development Zone, Chengdu, Sichuan, P. R. China.		Measurement Date	21/11/2024
Methods	IEC 60904-1:2020 Photovoltaic devices-Part 1: Measurement of Photovoltaic Current-Voltage Characteristics.			
Test conclusion	This column blank.			
Remarks	The mask area is provided by the Commission unit: 0.0374 cm ² .			
Approved by		Reviewed by		
		Measured by		

(Special chapter for test report)
Issue Date: 06/11/2024

Fig. S8 The certification test report of the best performance provided by National Photovoltaic Product Quality Inspection & Testing Center (Page 1 of the report).

Chengdu Institute of Product Quality Inspection Co., Ltd.
National Photovoltaic Product Quality Inspection & Testing Center
TEST REPORT

Test Report No. AGXB124W00743

Page 2 of 2

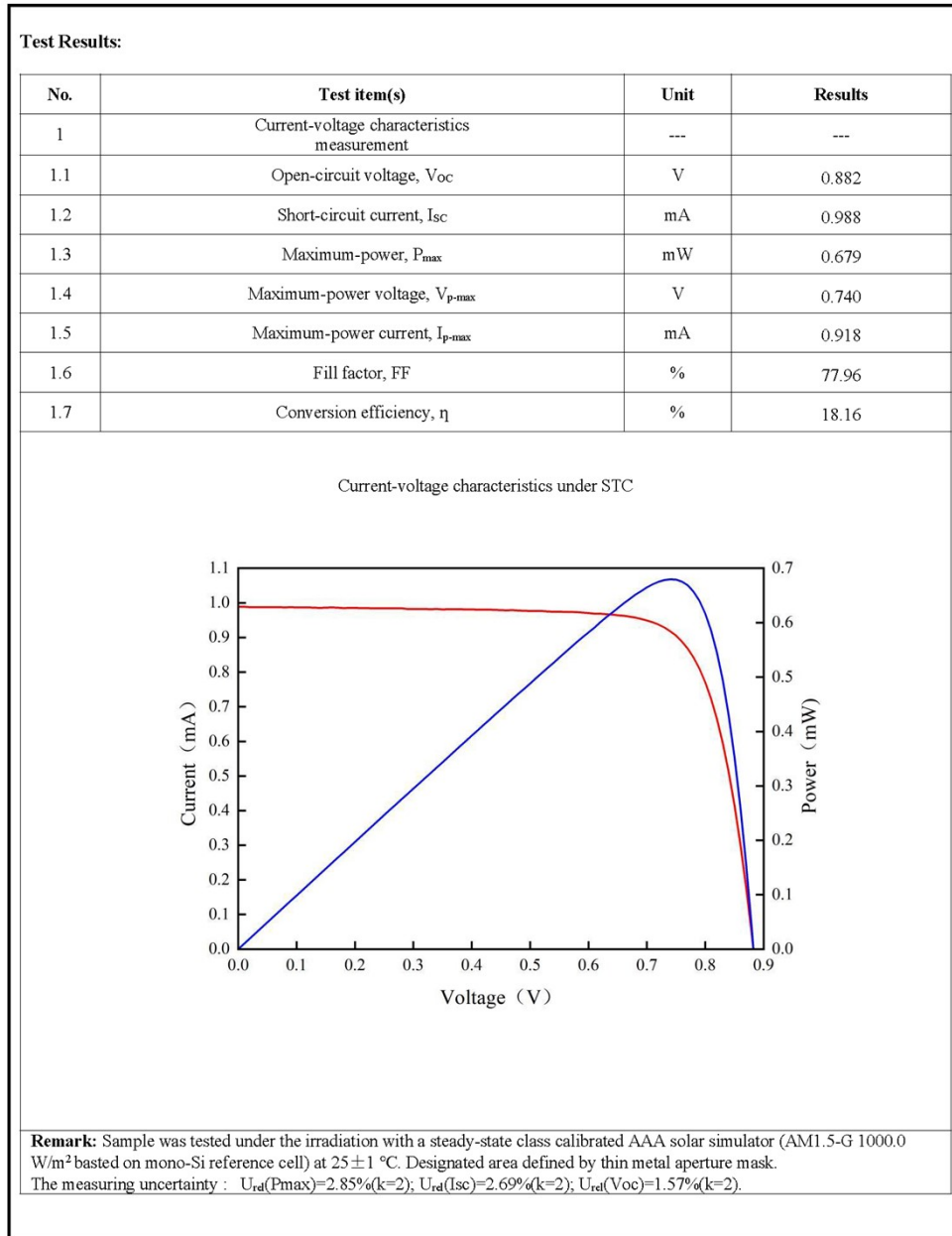


Fig. S9 The certification test report of the best performance provided by National Photovoltaic Product Quality Inspection & Testing Center (Page 2 of the report).

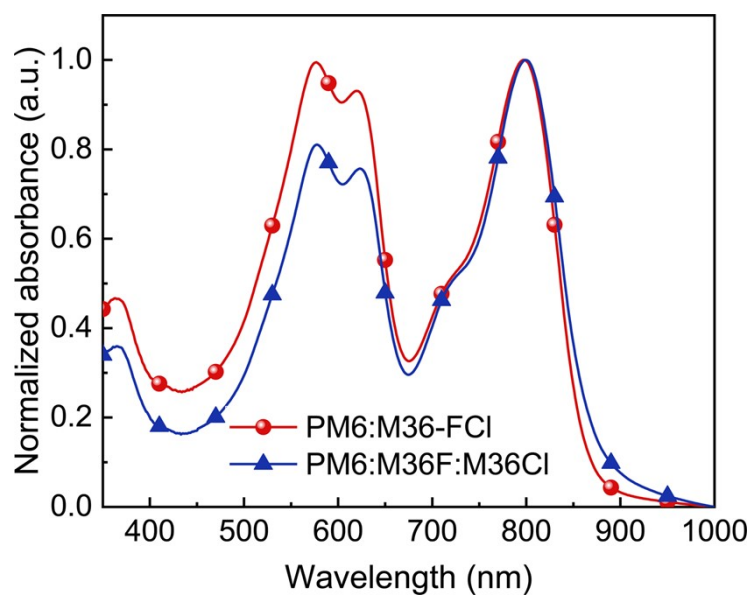


Fig. S10 Normalized thin-film absorption of the PM6:M36-FCI and PM6:M36F:M36Cl blend films.

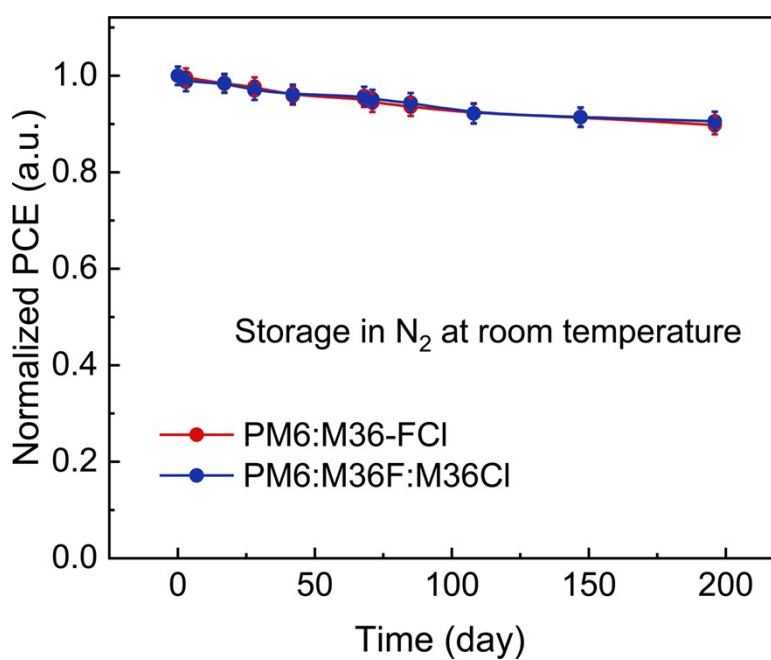


Fig. S11 Normalized PCEs of the PM6:M36-FCI- and PM6:M36F:M36Cl-based PSCs after storage at room temperature in a N₂-filled glovebox for different times.

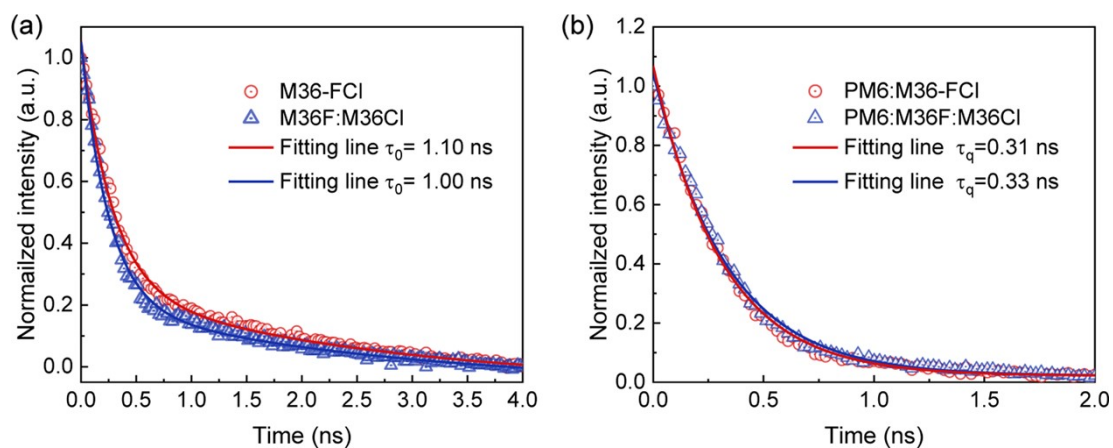


Fig. S12 (a) TRPL of M36-FCI and M36F:M36Cl films, which represent the respective singlet exciton lifetime (τ_0). (b) TRPL of PM6:M36-FCI and PM6:M36F:M36Cl blend films investigated in this study, which show the PL quenching lifetime in the BHJ (τ_q). The excitation wavelength was 800 nm for all the samples.

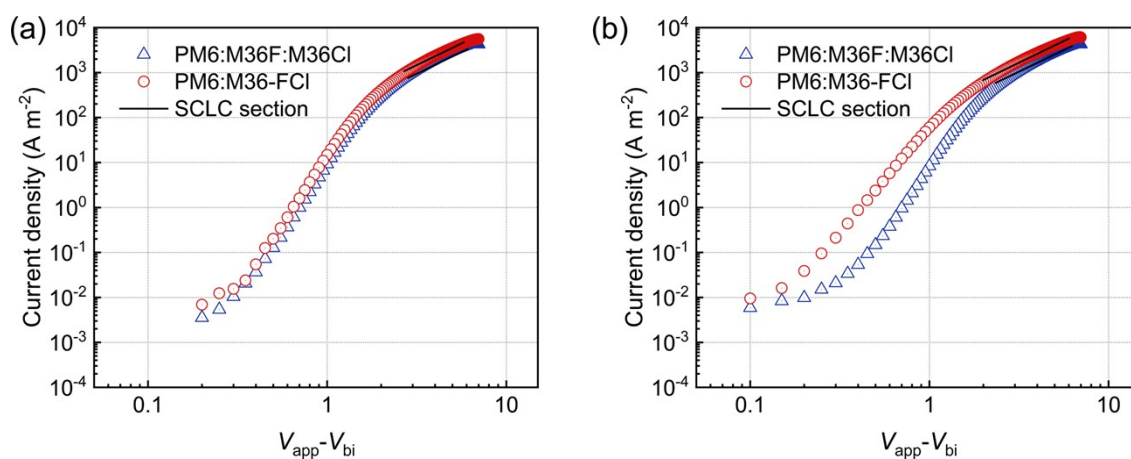


Fig. S13 J - V curves of (a) hole-only and (b) electron-only devices based on PM6:M36-FCI and PM6:M36F:M36Cl BHJ films under dark conditions.

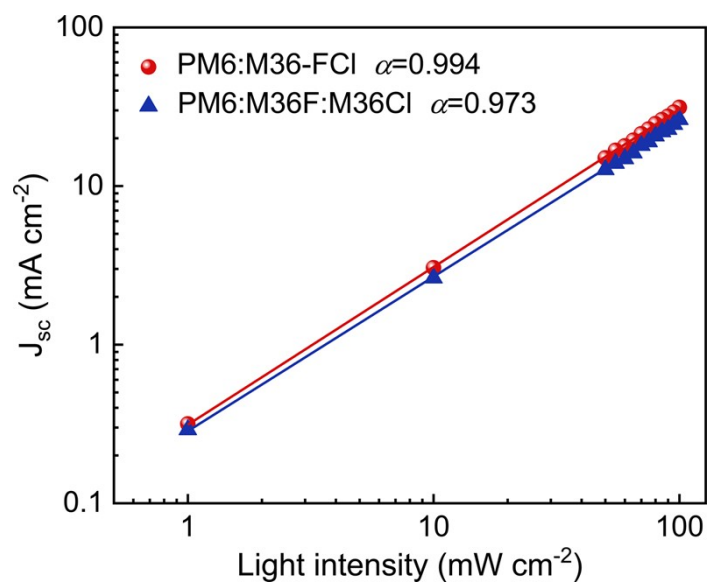


Fig. S14 J_{sc} - P_{light} characteristics of the optimized PSCs based on the PM6:M36-FCI and PM6:M36F:M36Cl BHJ films.

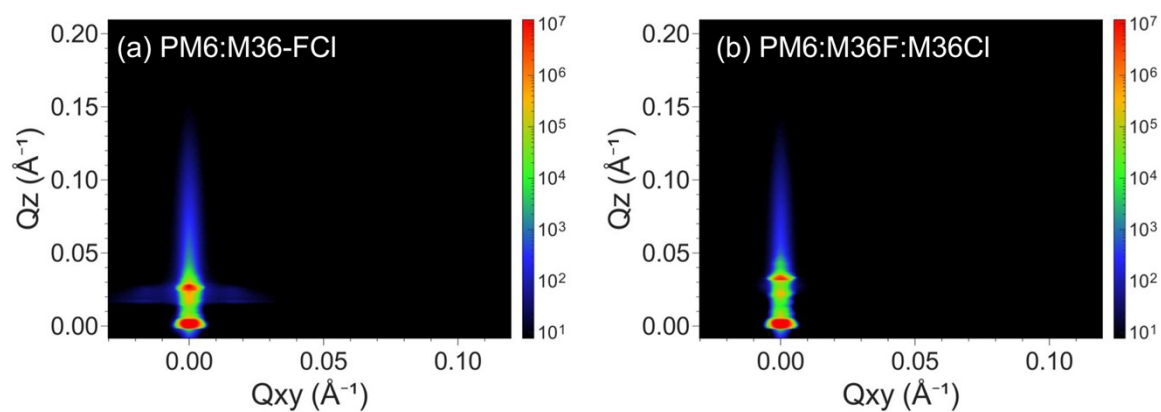


Fig. S15 2D GISAXS patterns of (a) PM6:M36-FCI and (b) PM6:M36F:M36Cl blend films.

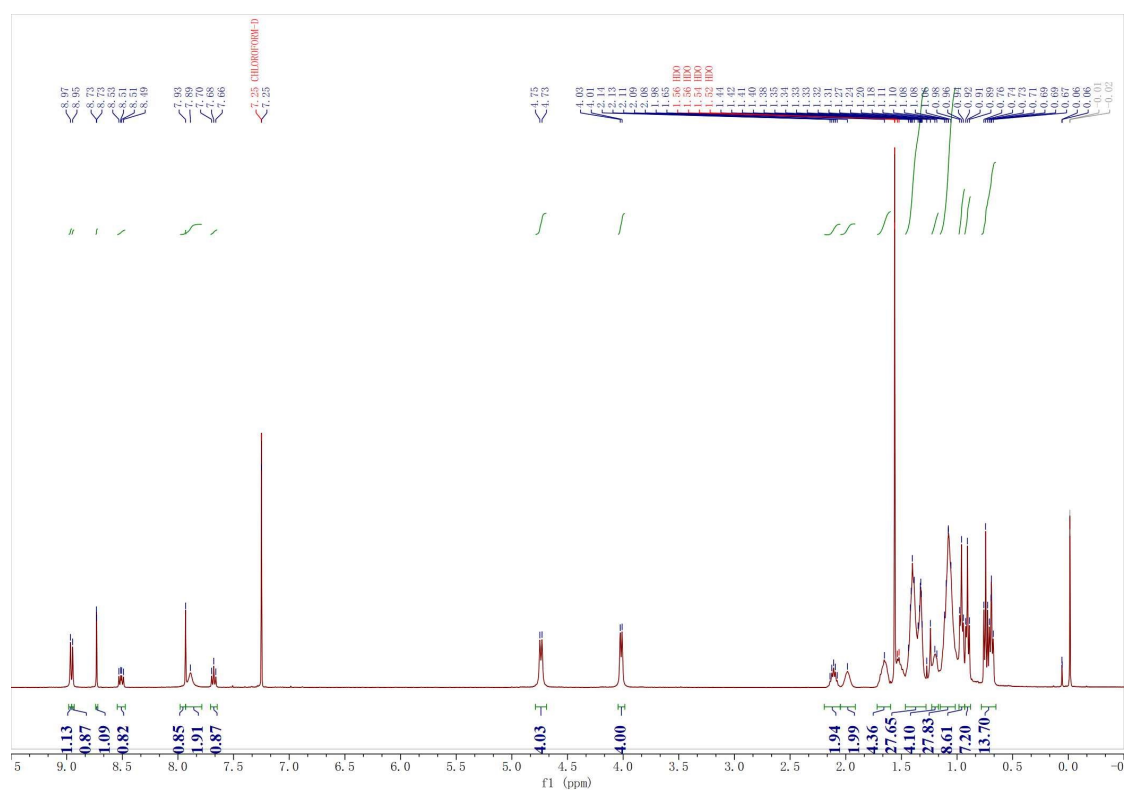


Fig. S16 ^1H NMR spectrum of M36-FCI.

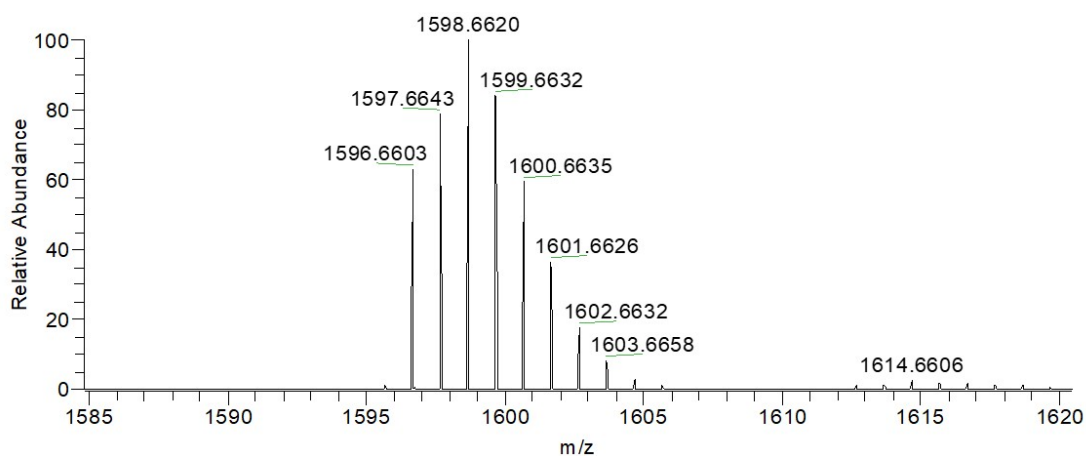


Fig. S17 HRMS spectrum of M36-FCI.

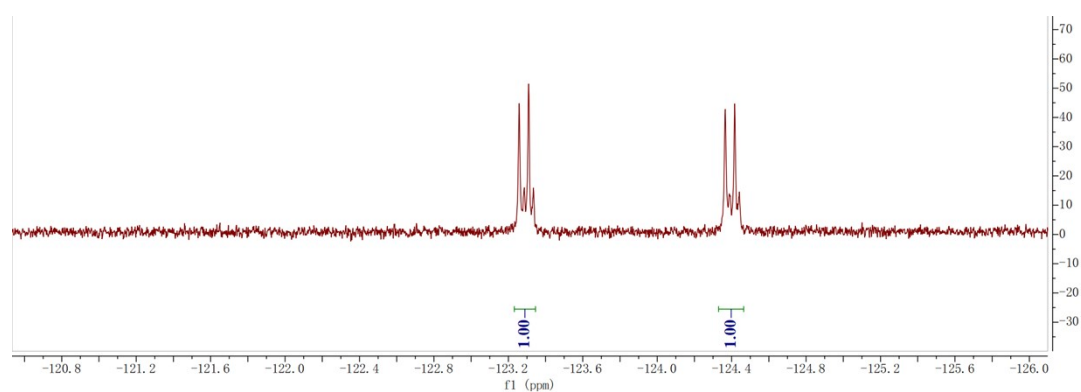


Fig. S18 ^{19}F NMR spectrum of M36-FCI.

References

- [S1] Y. Ma, M. Zhang, S. Wan, P. Yin, P. Wang, D. Cai, F. Liu and Q. Zheng, *Joule*, 2021, **5**, 197-209.
- [S2] Y. Lin, Y. Firdaus, F. H. Isikgor, M. I. Nugraha, E. Yengel, G. T. Harrison, R. Hallani, A. El-Labban, H. Faber, C. Ma, X. Zheng, A. Subbiah, C. T. Howells, O. M. Bakr, I. McCulloch, S. D. Wolf, L. Tsetseris and T. D. Anthopoulos, *ACS Energy Lett.*, 2020, **5**, 2935-2944.
- [S3] J. Fu, P. W. K. Fong, H. Liu, C.-S. Huang, X. Lu, S. Lu, M. Abdelsamie, T. Kodalle, C. M. Sutter-Fella, Y. Yang and G. Li, *Nat. Commun.*, 2023, **14**, 1760.
- [S4] M. P. Hughes, K. D. Rosenthal, N. A. Ran, M. Seifrid, G. C. Bazan and T.-Q. Nguyen, *Adv. Funct. Mater.*, 2018, **28**, 1801542.
- [S5] L. J. A. Koster, S. E. Shaheen and J. C. Hummelen, *Adv. Energy Mater.*, 2012, **2**, 1246-1253.
- [S6] Z. Chen, C. Yu, K. Shum, J. J. Wang, W. Pfenninger, N. Vockic, J. Midgley and J. T. Kenney, *J. Lumin.*, 2012, **132**, 345-349.
- [S7] X. Li, Y. Wu, S. Zhang, B. Cai, Y. Gu, J. Song and H. Zeng, *Adv. Funct. Mater.*, 2016, **26**, 2435-2445.